AEDC-TR-69-186

EXPERIMENTAL INVESTIGATION OF LAMINAR FLOW DEVELOPMENT IN A RECTANGULAR CHANNEL USING A LASER ANEMOMETER

W. T. Snyder and W. H. Goethert

ARO, Inc.

October 1969

ARNOLD ENGINEERING DEVELOPMENT CENTER
AIR FORCE SYSTEMS COMMAND
ARNOLD AIR FORCE STATION, TENNESSEE

PROPERTY OF U. S. AIR FORCE
AEDC LIBRARY
F40600-69-C-0001

NOTICES

When U. S. Government drawings specifications, or other data are used for any purpose other than a definitely related Government procurement operation, the Government thereby incurs no responsibility nor any obligation whatsoever, and the fact that the Government may have formulated, furnished, or in any way supplied the said drawings, specifications, or other data, is not to be regarded by implication or otherwise, or in any manner licensing the holder or any other person or corporation, or conveying any rights or permission to manufacture, use, or sell any patented invention that may in any way be related thereto.

Qualified users may obtain copies of this report from the Defense Documentation Center.

References to named commercial products in this report are not to be considered in any sense as an endorsement of the product by the United States Air Force or the Government.

EXPERIMENTAL INVESTIGATION OF LAMINAR FLOW DEVELOPMENT IN A RECTANGULAR CHANNEL USING A LASER ANEMOMETER

W. T. Snyder* and W. H. Goethert
ARO, Inc.

*Consultant, ARO, Inc., Professor of Aerospace Engineering, The University of Tennessee Space Institute

FOREWORD

The work reported herein was done at the request of Headquarters, Arnold Engineering Development Center (AEDC), Air Force Systems Command (AFSC), under Program Element 65401F, Project 4344, Task 32.

The results of research presented were obtained by ARO, Inc. (a subsidiary of Sverdrup & Parcel and Associates, Inc.), contract operator of AEDC, AFSC, Arnold Air Force Station, Tennessee, under Contract F40600-69-C-0001. The research was conducted under ARO Project No. BC5919, and the manuscript was submitted for publication on July 29, 1969.

The authors wish to acknowledge the invaluable assistance given to the experimental phase of this investigation by co-op student, Mr. H. Blackburn.

This technical report has been reviewed and is approved.

David G. Francis
1st Lt, USAF
Research Division
Directorate of Plans
and Technology

Harry L. Maynard
Colonel, USAF
Director of Plans
and Technology

ABSTRACT

Flow in the entrance region of a parallel plate channel has been theoretically investigated by others with little or no experimental verification. Presented here is a new method for the analysis which involves a linearization of the inertia terms and the introduction of a stretched axial coordinate. Solutions are obtained for the velocity distribution in an incompressible fluid which is valid from the duct inlet to the fully developed region. An experimental parallel plate channel was operated using water as the working fluid. Velocity profiles, on the basis of the stretched axial coordinate, were established with the use of a laser doppler velocimeter. These velocity profiles are compared with the theoretical profiles. A significant variation between the experimental and theoretical velocity is seen near the inlet of the channel.

CONTENTS

APPENDIXES

I. ILLUSTRATIONS

Figure

II. TABLES

SECTION I
INTRODUCTION

A significant portion of the flow variations, particularly with short length channels, is experienced in the entrance region. For a constant property fluid, these variations exist until ultimately a velocity profile is attained which does not vary with axial position. Because of the influence of viscosity, the initial profile at the channel entrance will be modified with respect to axial position until this fully developed profile is achieved.

A number of theoretical investigations of flow development in the entrance region of channels have been made, but the experimental data available are meager. A summary of the various analytical approaches to the entrance region problem is presented by Sparrow, Lin, and Lundgren (Ref. 1). These authors developed a new method of flow analysis in the entrance region and compared their results with the small amount of experimental data which was available. The only experimental data cited were for flow in a circular tube. The linearized analysis developed by Sparrow et al. gave better agreement with the available experimental data than the other analyses that were cited.

Recent experimental measurements of velocity profiles in the entrance region of a square duct have been made by Goldstein and Kreid (Ref. 2) using a laser-doppler flowmeter. The experimental results were compared with the theoretically calculated profiles of Han (Ref. 3). The analysis of Han is based on a Langhaar (Ref. 4) method of linearization. However, it has been shown (Ref. 1) that the Langhaar method predicts a more rapid development of the entrance region flow than the rate predicted by the linearization method when compared with the experimentally measured rate of development. The experimental data (Ref. 2) agreed well with the theoretical calculations in the fully developed portion of the channel, but variations existed between the theoretical and experimental values as one approached the entrance region. The variations between the theoretical and experimental values increased with decreasing distance to the entrance region.

In the present investigation, measurements of velocity profiles in the entrance region of a rectangular channel were made with a helium-neon gas laser anemometer. The channel had an aspect ratio of 7.4 to 1. A comparison was made between the experimental measurements and profiles calculated using the linearization method of Sparrow, Lin, and Lundgren described in Ref. 1. The principal objectives were to determine the validity of the analytical model described in Ref. 1 and to obtain

measured velocity profiles in the entrance region of a rectangular channel using a laser anemometer.

SECTION II
ANALYSIS

In analyzing entrance region flows, two levels of approximation are generally involved, and the distinction between them is not always made clear. The flow in the entrance region is described exactly by the complete Navier-Stokes equations (for continuum flow). The Navier-Stokes equations are elliptic, and this means that boundary conditions must be specified at each point around a closed contour. Thus, in addition to prescribing a profile at the entrance to the channel at $x = 0$, the profile must also be specified at $x = \infty$. Since the boundary-layer equations are parabolic, the equations may be integrated in a forward marching manner by starting with a prescribed initial profile at $x = 0$. Thus, the first level of approximation involves the use of the boundary-layer form of the equations of motion instead of the full Navier-Stokes equations, thereby changing the system from elliptic to parabolic. Any analysis of entrance region flows based on the boundary-layer equations will be invalid at the channel entrance because of the neglect of the term $\partial^2 u/\partial x^2$, which is not small at the entrance.

The second level of approximation is involved in the particular technique used to solve the boundary-layer equations. Several approximate methods have been used to solve the boundary-layer equations; however, in the present analysis the approximate linearization method (Ref. 1) was used. This method was chosen because it appeared to give the best agreement with the available experimental data. The analysis is performed for a parallel plate channel geometry.

The geometry of the parallel plate channel is shown in Fig. 1 (Appendix I). The boundary-layer form of the equation of motion for the entrance region flow of a constant property, incompressible fluid may be written as

$$u \frac{\partial u}{\partial x} + v \frac{\partial u}{\partial y} = - \frac{1}{\rho} \frac{\partial p}{\partial x} - \nu \frac{\partial^2 u}{\partial y^2} \qquad (1)$$

Because of the nonlinearity of Eq. (1), an exact solution is not possible. Following the linearization technique described in Ref. 1, Eq. (1) is linearized as:

$$\epsilon(x)U\frac{\partial u}{\partial x} = \Lambda(x) + \nu\frac{\partial^2 u}{\partial y^2} \tag{2}$$

where $\epsilon(x)$ is a stretching factor and U is the mean velocity defined as

$$U = \frac{1}{h}\int_0^h u\,dy \tag{3}$$

The term $\Lambda(x)$ contains the pressure gradient and the residual of the inertia terms and may be evaluated by integrating Eq. (2) over the channel half-width with the result

$$\Lambda(x) = -\left[\frac{\nu}{h}\frac{\partial u}{\partial y}\right]_{y=h} \tag{4}$$

Combining Eqs. (2) and (4) gives

$$\epsilon(x)U\frac{\partial u}{\partial y} = \nu\left\{\frac{\partial^2 u}{\partial y^2} - \left[\frac{1}{h}\frac{\partial u}{\partial y}\right]_{y=h}\right\} \tag{5}$$

A stretched coordinate x* may be introduced by the definition

$$dx = \epsilon dx^*$$

which transforms the left side of Eq. (5) to a form with a constant coefficient

$$\epsilon(x)U\frac{\partial u}{\partial x} = U\frac{\partial u}{\partial x^*} \tag{6}$$

Dimensionless quantities may be defined as follows:

$$a = \frac{u}{U},\ \eta = \frac{y}{h},\ \beta^* = \frac{x^*}{h}\left(\frac{1}{Re}\right),$$

$$\beta = \frac{x}{h}\left(\frac{1}{Re}\right),\ Re = \frac{hU}{\nu} \tag{7}$$

The dimensionless form of the equation of motion becomes

$$\frac{\partial a}{\partial \beta^*} = \frac{\partial^2 a}{\partial \eta^2} - \left[\frac{\partial a}{\partial \eta}\right]_{\eta=1} \tag{8}$$

with boundary conditions

$$a(0,\eta) = a_o(\eta);\ a(\beta,1) = 0;\ \frac{\partial a}{\partial \eta}(\beta;0) = 0 \tag{9}$$

For a uniform initial velocity profile, $a_o(\eta) = 1$. The solution to Eq. (7), subject to the boundary conditions of Eq. (8) and $a_o(\eta) = 1$, is given as (Ref. 1):

$$a = \frac{3}{2}(1 - \eta^2) + \sum_{n=1}^{\infty}{}' \frac{2}{\gamma^2_n}\left\{\frac{\cos \gamma_n \eta}{\cos \gamma_n} - 1\right\} \exp\left(-\gamma^2_n \beta^*\right) \tag{10}$$

where γ_n are eigenvalues which are the roots of the transcendental equation

$$\gamma_n = \tan \gamma_n \tag{11}$$

The first 98 eigenvalues of Eq. (10) were evaluated (Ref. 5) and are tabulated in Table I (Appendix II).

To complete the analysis, the stretching factor $\epsilon(x^*)$ must be determined. The procedure developed in Ref. 1 is to integrate the equation of motion across the half-channel and then to integrate the first moment of the equation motion, i.e., the integral of the velocity, u, times the equation of motion. Equating the pressure gradient obtained from the two equations then results in a solution for ϵ of the form

$$\epsilon(\beta^*) = \frac{\int_0^1 \left(2a - \frac{3}{2}a^2\right)\frac{\partial a}{\partial \beta}\, d\eta}{\left[\frac{\partial a}{\partial \eta}\right]_{\eta=1} + \int_0^1 \left(\frac{\partial a}{\partial \eta}\right)^2 d\eta} \tag{12}$$

It should be observed that the evaluation of $\epsilon(\beta^*)$ as given by Eq. (12) is not unique since other moments of the equation of motion could be used as well. There appears to be no compelling physical reason for using moments higher than the zeroth and first, and consequently these two moments were used to climinate the pressure gradient from the equation of motion, resulting in a solution for $\epsilon(\beta^*)$.

The integrals appearing in Eq. (12) were evaluated numerically using an IBM 360/50 digital computer. From the calculated values of $\epsilon(\beta^*)$, the relation between the physical and stretched coordinates may be obtained from the definition of ϵ as

$$\frac{x}{h} = Re_0 \int^{\beta^*} \epsilon d\beta^* \qquad (13)$$

Thus, Eqs. (9), (11), and (12) constitute the solution for the entrance region velocity profile based on the linearization model described by Sparrow et al. (Ref. 1).

Figure 2 is a plot of β versus β^* obtained from the solution of Eq. (13). Figure 3 is a plot of α and $\partial\alpha/\partial\beta^*$ versus β^* evaluated at the centerline obtained from Eq. (9). These two quantities will be useful in performing an error analysis which will be described later.

SECTION III
DESCRIPTION OF EXPERIMENTAL APPARATUS

To determine the validity of the above theoretical analysis, an experimental channel flow facility was designed and built which would permit measurement of entrance region velocity profiles using a laser anemometer. The flow system shown schematically in Fig. 4 consists of a constant head reservoir which feeds a plenum chamber. From the plenum chamber the flow enters a 2-m-long developing section which allows the flow to become fully developed before the initial conditioning section is entered. The developing section was added because of the extreme difficulty encountered in obtaining a constant initial velocity profile entering the test section. Since the velocity profile existing from this section is the well-known Poiseuille profile, various schemes for obtaining a flat profile at the entrance to the test section could be studied with a minimum of difficulty. Beyond the developing section the flow passes through a screen diffuser with a solidity ratio of 0.162, i.e., $1 - A_o/A_t$ when A_o is the open area of the screen and A_t is the total area of the screen, and into the test section which consists of two rectangular glass channels, one inside the other. The dimensions are 14 by 3.8 cm for the outer channel and 14 by 1.9 cm for the inner channel. The purpose of the inner channel is to allow only the flat central portion of the channel profile to enter the test section, thus resulting in a well-defined flat initial profile. The length of the test section is 76 cm. The leading edges of the inner channel are slightly rounded to minimize flow separation. The data presented were for the flow within the inside channel. The flow from the test section then enters a dump tank where it is returned to the reservoir by the secondary loop shown in Fig. 4. It was found necessary to vent the flow system to remove fluctuations caused by air bubbles trapped during the filling process.

The laser anemometer system, shown schematically in Fig. 1, has a traverse capability across the channel and down the length of the channel so that velocity profiles can be obtained at different stages of flow development. The anemometer incorporates the doppler shift effect with optical homodyne detection similar to that used by Yeh and Cummins (Ref. 6).

SECTION IV
INITIAL CONDITION

Considerable effort was expended to obtain a flat velocity profile at the beginning of the knife edges of the test channel. Figure 5 is a superimposed plot of the velocity profile immediately upstream and downstream of the straightening screen. The upstream profile is parabolic, as would be expected since the flow has passed through the 2-m developing section. The downstream profile exhibits a marked concavity on the centerline. It was found that a very minute deflection in the center of the straightening screen was the apparent reason for the inflection. The screen holder was redesigned so that the screen could be put under considerable tension to avoid the deflection. The resulting profile downstream of the new screen arrangement is shown in Fig. 6. This is a typical initial profile obtained for all the experiments that were conducted. The location of the knife edges relative to the profile is also shown in Fig. 6.

SECTION V
ANALYSIS OF THE EXPERIMENTAL DATA

Since the doppler frequency is directly proportional to the longitudinal component of velocity, for the optical configuration used in this study, normalized velocity profiles were obtained by numerical integration of the doppler frequency shift profiles. The normalized profiles across the channel were obtained by dividing the locally measured frequency by the average frequency over the channel width and normalized to the center velocity at the entrance of the channel; hence, the center, fully developed Poiseuille velocity becomes 1.5. Figure 7 is a plot of several normalized velocity profiles obtained in this manner using β^* as a parameter. By using β^* as a parameter, one may make all measurements at one downstream position, x, and vary the flow rate (Reynolds number) to produce the equivalent developing profile. The Reynolds number used to calculate β^* was obtained from flow rate measurements determined by volumetric means. It is apparent that the measured and

calculated profiles are in close agreement near the fully developed region (large values of β^*). Near the entrance, however, the measured centerline velocities are consistently lower than the calculated values. To check the value of β^* obtained from the volumetric measurements, the average doppler frequency was converted to the flow rate and compared with the volumetric flow rate. The doppler frequency is given by

$$f_D = \frac{2nV}{\lambda_o} \sin \frac{\theta}{2} \cos \frac{\theta}{2} \tag{14}$$

where f_D is the frequency measured, V is the velocity, n is the index of refraction, and θ is the angle between scattered beam and reference beam. The laser wavelength is λ_o. The mass flow rate $\dot{W}$ is given by

$$\dot{W} = \langle V \rangle A \tag{15}$$

with A being the cross-sectional area of the test section and where $\langle V \rangle$ is the average velocity or bulk velocity.

Since the average velocity is directly proportional to the average doppler shifted frequency, $\dot{W}$ may be found. The average frequency was established from a computer program which provided an analytic equation for each velocity profile (frequency profile) and performed the following integration,

$$\langle f \rangle = \frac{1}{A} \iint f \, dA$$

With the use of the average frequency in Eq. (14) and substituting into Eq. (15), we have

$$\dot{W} = \frac{\langle f_D \rangle \lambda_o A}{2n \sin\left(\frac{\theta}{2}\right) \cos\left(\frac{\theta}{2}\right)} \tag{16}$$

The angle θ was found with the use of Snell's law (also see Fig. 1)

$$n_1 \sin \theta_1 = n_2 \sin \theta_2 \tag{17}$$

where n_1 and n_2 were the index of refraction of the water and air, respectively. Since the data were taken over a period of several days, a

new θ_2 was found each day to ensure high accuracies. Then θ_1 was calculated with n = 1 and n_2 = 1.35 such that

$$\theta_1 = \sin^{-1}\left[\frac{\sin\theta_2}{1.35}\right] \tag{18}$$

Table II contains the flow rate obtained in this manner along with those obtained from the volumetric measurements. Except for run 1, it is seen that the laser anemometer values are consistently lower than the volumetric measured values. Hence, the values of β^* calculated from Reynolds numbers based on the anemometer measurements would then be larger than those from the volumetric measurements by an average of 2.8 percent. Since the normalized centerline velocity increases with increasing β^*, profile comparisons based on the anemometer β^*'s would show an even worse correlation near the entrance. The shape of the measured profile indicates that the disagreement might be explained in terms of an error in the flow rate measurement, which would in turn produce an error in β^*.

To check this possibility, an error analysis of the centerline velocity determination attributable to an error in the measured flow rate was performed. The error in centerline velocity owing to an error in β^* is given by

$$(\Delta a)_{cl} = \left(\frac{\partial a}{\partial \beta^*}\right)_{cl} \Delta\beta^* \tag{19}$$

From the definition of β^*, Eq. (7), the error in the calculated β^* produced by an error in measured flow rate is given by

$$\Delta\beta^* = -\beta^* \frac{\Delta Re}{Re^2} \approx -\beta^* \frac{\Delta \dot{W}}{\dot{W}} \tag{20}$$

providing the increment is small compared to the absolute magnitude. Thus,

$$(\Delta a)_{cl} = -\left(\frac{\partial a}{\partial \beta^*}\right)_{cl} \beta^* \frac{\Delta \dot{W}}{\dot{W}} \tag{21}$$

The derivative was found by plotting β^* versus the experimental centerline velocity and then performing a graphical differentiation of this plot. The results are reproduced in Fig. 3.

The percentages of error between the theoretical and experimental data of the β^*'s associated with the normalized velocity profiles shown in Fig. 7 are tabulated in Table III. In addition, the table includes the error between the anemometer and volumetric flow rates, assuming the anemometer measurements were correct. These experimental flow rate errors were used in Eq. (21) to determine the approximate error in the centerline velocity. The results are tabulated in the last column of Table III. It is seen that this error is negligible compared with the error between the experimental and theoretical data.

Several sources of error are attributable to the laser anemometer, but these errors may be assumed to be quite small. These errors are inherent in determining the angle θ_2 (or the ability to measure the three sides of a triangle accurately), the ability of determining the mean velocity of a Gaussian velocity distribution, and the ability to measure frequency accurately. These errors were found to be less than 0.5 percent; hence, they contributed little or no error in β^*. The location of the position x^* was found within 0.0001 in.

At this time, it may be assumed that the gradual increase in variation that is found by approaching the channel entrance is caused by insufficiencies in the theoretical model on which the analysis is performed.

SECTION VI
CONCLUSIONS

The velocity profiles in the entrance region of a rectangular flow channel were measured with a laser anemometer. The measurements were compared with profiles calculated by a method developed by Sparrow. Satisfactory agreement was found near the fully developed region, but deviations were noted close to the entrance which cannot be accounted for by experimental error. It is concluded from the experimental data that the theory used accurately predicts entrance region profiles for distances from the channel entrance such that $x/h > (0.025/Re)$. For distances smaller than this, the theory predicts a more rapid development of the flow than is measured experimentally. This is thought to be an inadequacy in the analytical model very near the entrance. Since the model used in the analysis is of the boundary-layer type, a discrepancy between theory and experiment would be expected very near the entrance because of the neglect of the $\partial^2 u/\partial x^2$ term in the boundary-layer equation.

REFERENCES

1. Sparrow, E. M., Lin, S. H., and Lundgren, T. S. "Flow Development in the Hydrodynamic Entrance Region of Tubes and Ducts," Physics of Fluids. Vol. 7, No. 3, March 1964, pp. 338-347.

2. Goldstein, R. J. and Kreid, D. K. "Measurement of Laminar Flow Development in Square Duct Using Laser-Doppler Flowmeter," Journal of Applied Mechanics. December 1967, pp. 813-818.

3. Han, L. S. "Hydrodynamic Entrance Lengths for Incompressible Laminar Flow in Rectangular Ducts," Journal of Applied Mechanics. September 1960, pp. 403-409.

4. Langhaar, H. L. "Steady Flow in the Transition Length of a Straight Tube," Journal of Applied Mechanics. June 1942, pp. 55-58.

5. Snyder, W. T. and Eraslan, A. H. "The Influence of Hall Effect and Initial Velocity Profile on MHD Flow in the Entrance Region of a Parallel Plate Channel." AEDC-TR-67-79 (AD650820), April 1967.

6. Yeh, Y. and Cummins, H. Z. "Localized Fluid Flow Measurements with He-Ne Laser Spectrometer," Applied Physics Letters. Vol. 4, No. 10, May 1964, pp. 176-178.

APPENDIXES

I. ILLUSTRATIONS

II. TABLES

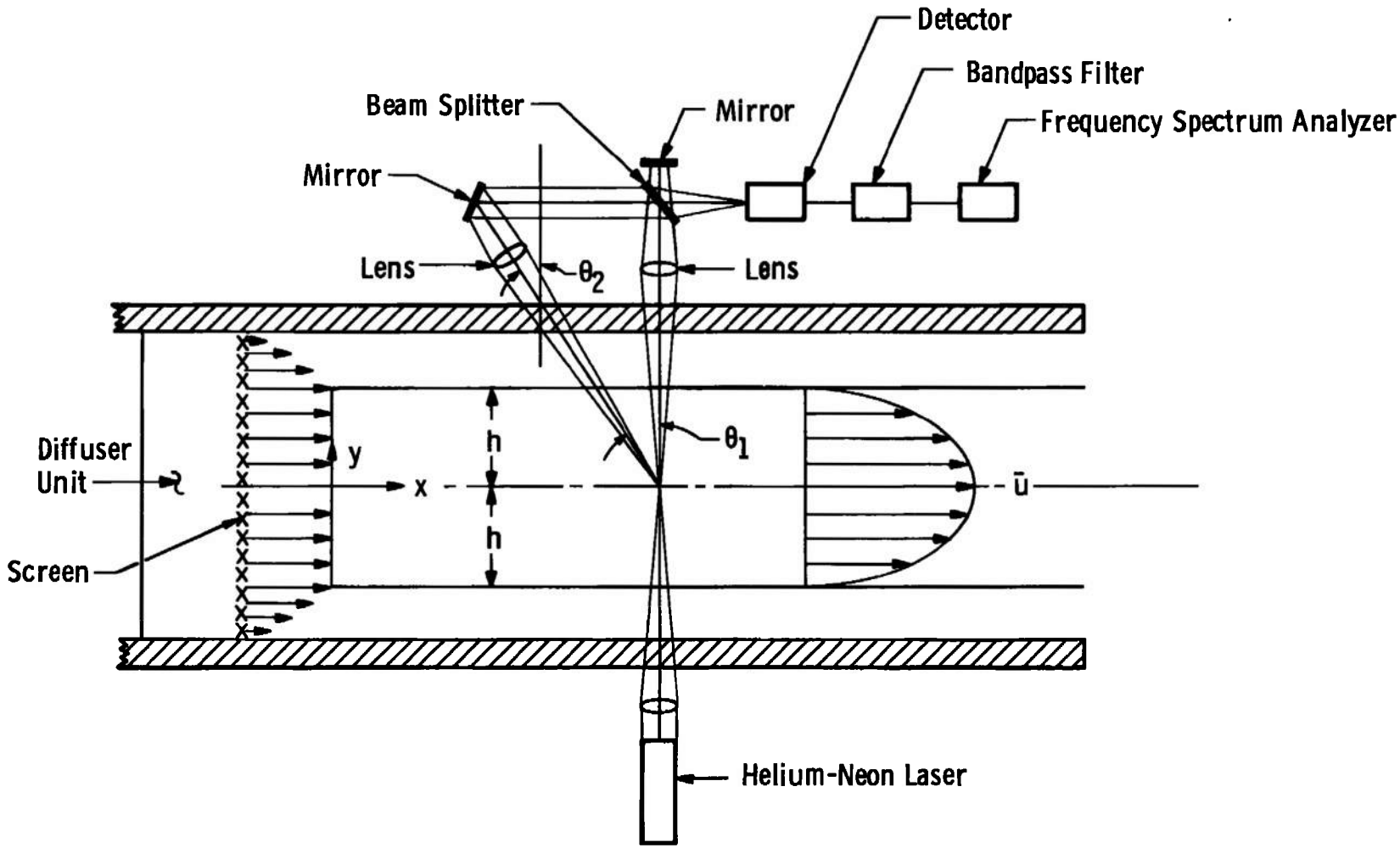

Fig. 1 Parallel Plate Geometry and Optical Arrangement

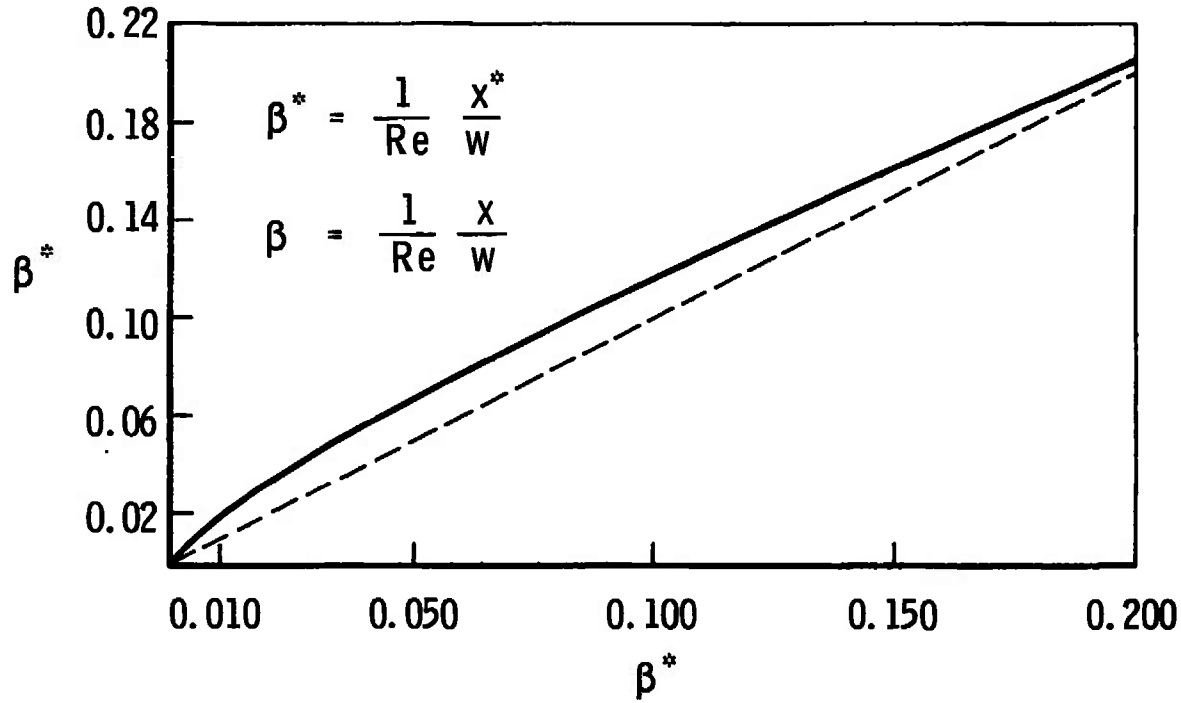

Fig. 2 B versus β^*

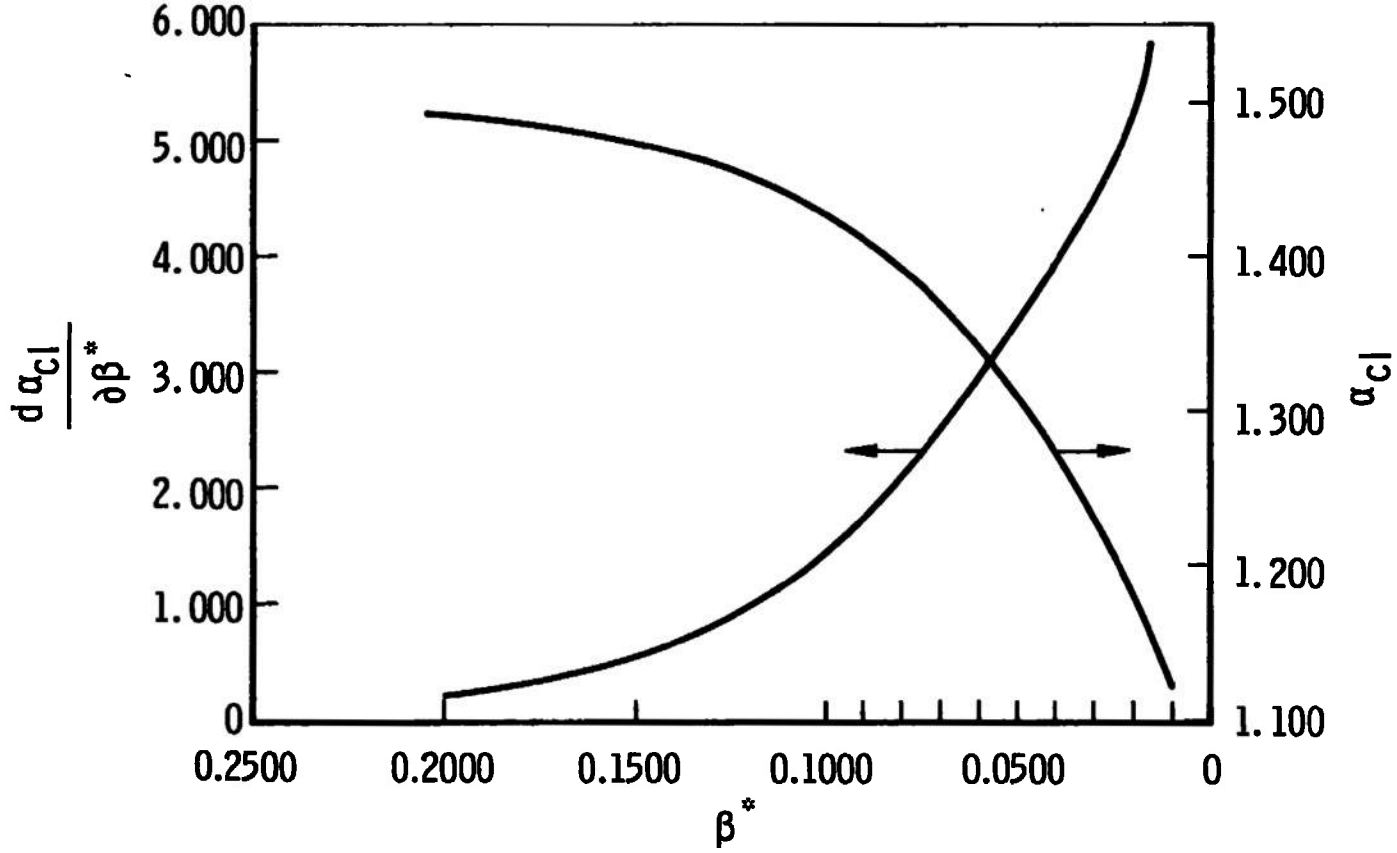

Fig. 3 Centerline Velocity and Derivotive of Centerline Velocity versus β^*

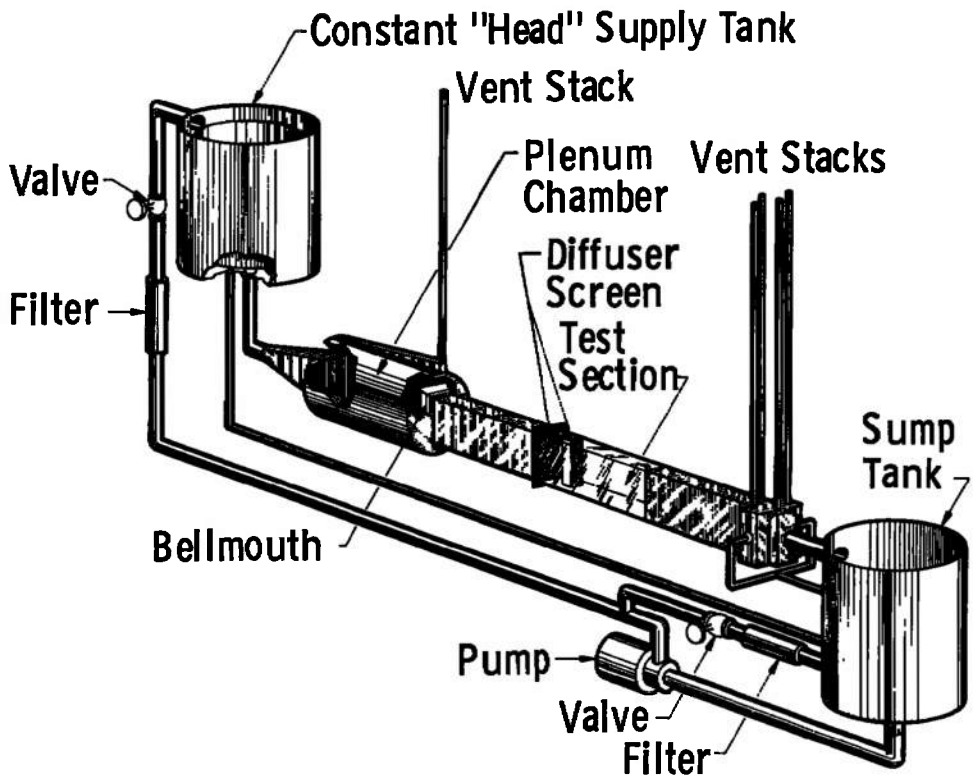

Fig. 4 Schematic Diagram of Flow System

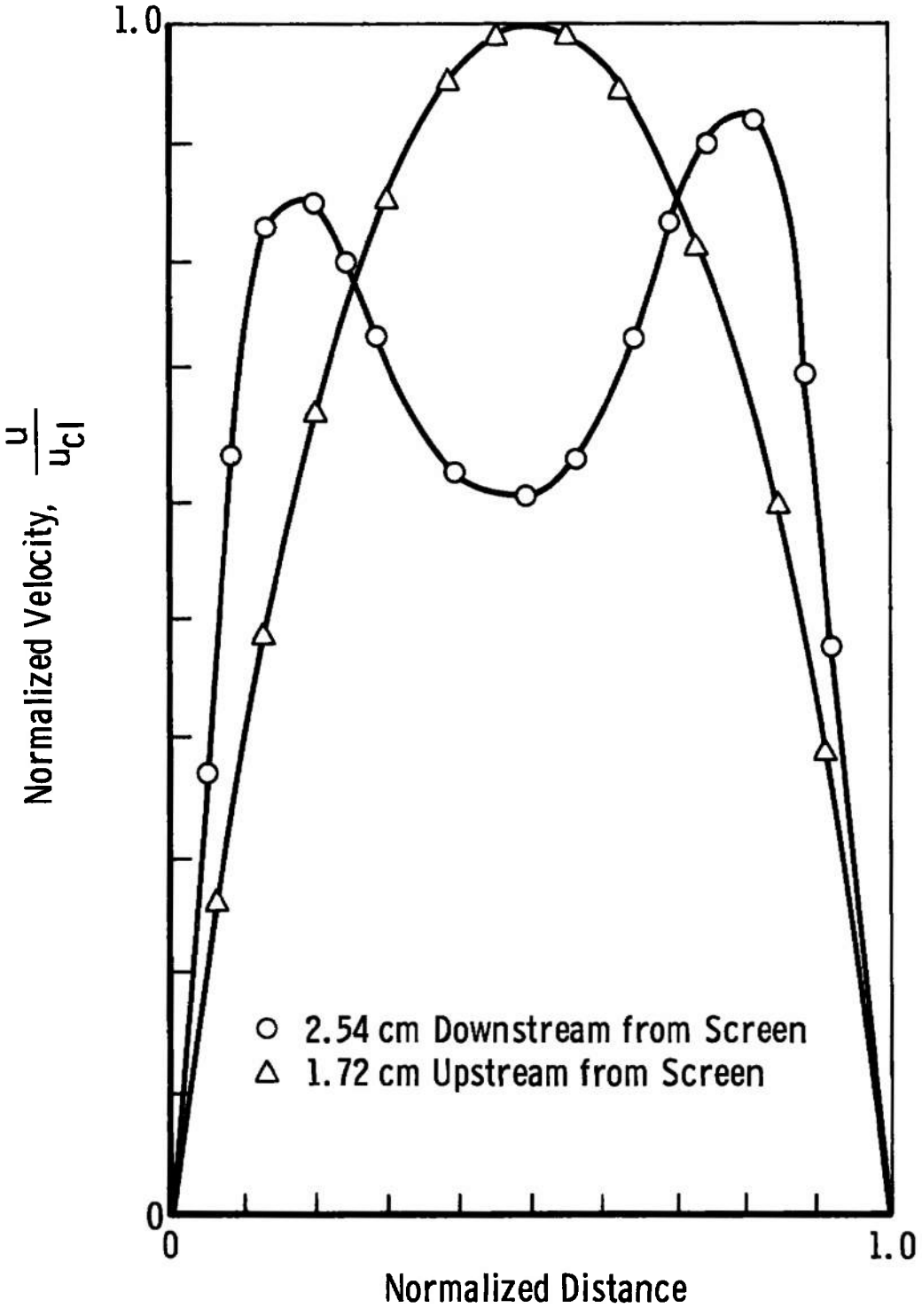

Fig. 5 Velocity Profiles of Upstream and Downstream Sides of a Slightly Deformed Diffuser Screen

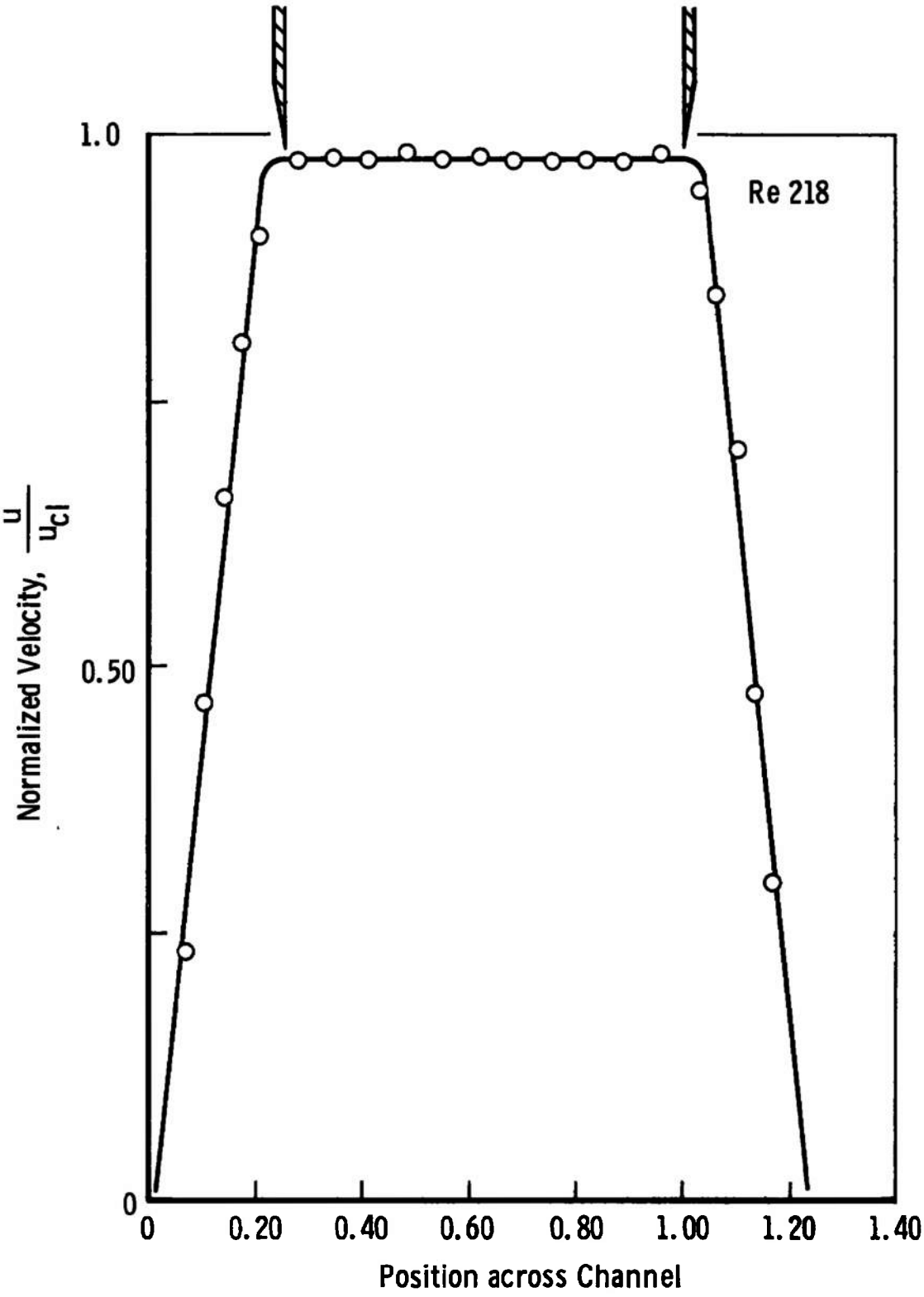

Fig. 6 Velocity Profile near Entrance of Test Section

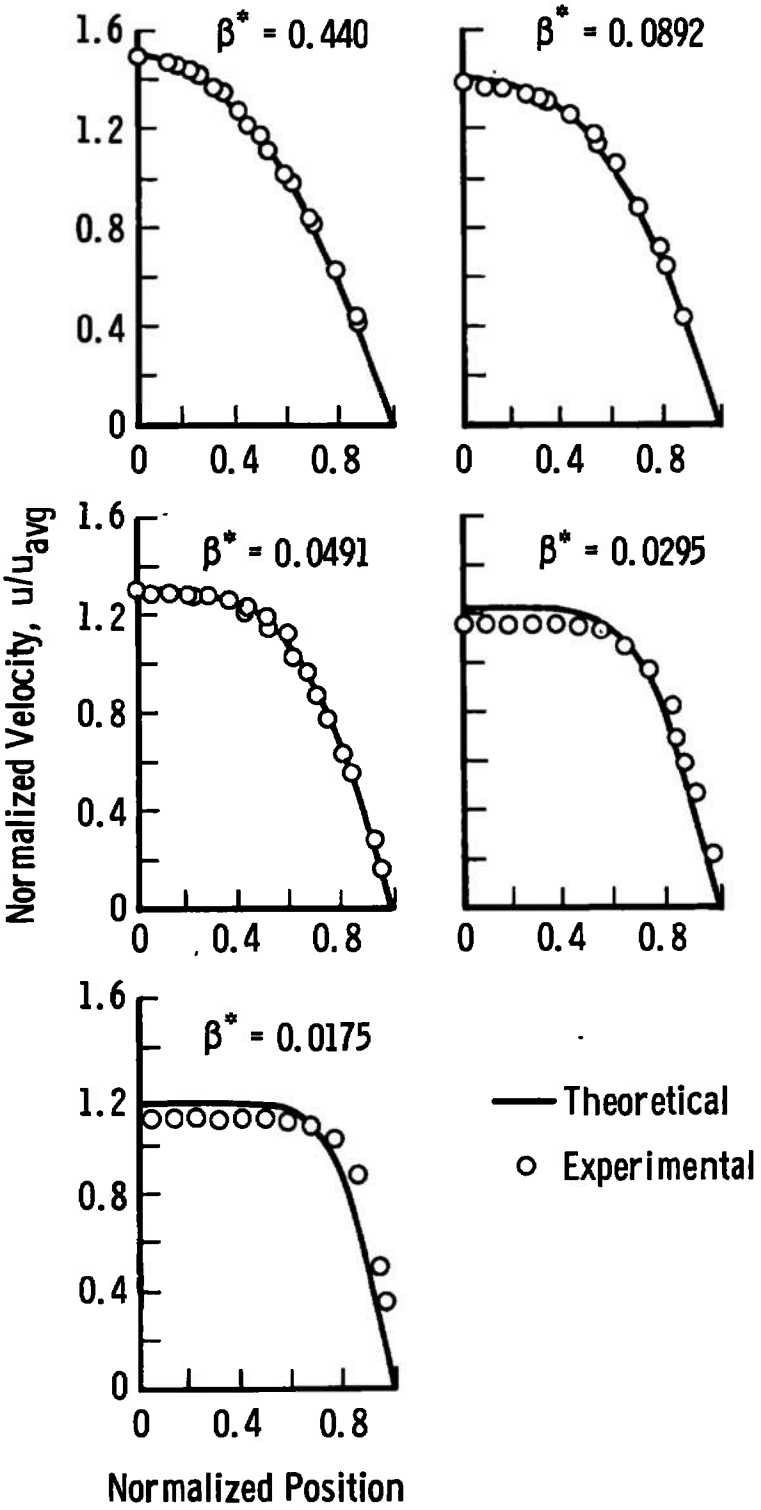

Fig. 7 Normolized Velocity Profiles versus Normalized Position

TABLE I
EIGENVALUES OF TAN $\gamma_n = \gamma_n$

n	γ_n	n	γ_n	n	γ_n
1	4.4934127	33	105.23392	66	208.91127
2	7.7252596	34	108.37579	67	212.05293
3	10.904133	35	111.51764	68	215.19459
4	14.066202	36	114.65947	69	218.33625
5	17.220769	37	117.80130	70	221.47790
6	20.371314	38	120.94311	71	224.61956
7	23.519473	39	124.08491	72	227.76121
8	26.666072	40	127.22676	73	230.90286
9	29.811615	41	130.36854	74	234.04451
10	32.956418	42	133.51031	75	237.18616
11	36.100648	43	136.65207	76	240.32781
12	39.244457	44	139.79383	77	243.46945
13	42.387936	45	142.93557	78	246.61109
14	45.531176	46	146.07731	79	249.75286
15	48.674183	47	149.21905	80	252.89450
16	51.817019	48	152.36077	81	256.03613
17	54.959713	49	155.50250	82	259.17777
18	58.102287	50	158.64422	83	262.31941
19	61.244761	51	161.78593	84	265.46104
20	64.387179	52	164.92764	85	268.60268
21	67.529490	53	168.06935	86	271.74431
22	70.671740	54	171.21104	87	274.88594
23	73.813931	55	174.35274	88	278.02757
24	76.956076	56	177.49453	89	281.16920
25	80.098176	57	180.63621	90	284.31083
26	83.240237	58	183.77789	91	287.45246
27	86.382265	59	186.91958	92	290.59408
28	89.524307	60	190.06126	93	293.73571
29	92.666274	61	193.20293	94	296.87734
30	95.808220	62	196.34460	95	300.01897
31	98.950141	63	199.48627	96	303.16059
32	102.09204	64	202.62794	97	306.30222
		65	205.76961	98	309.44384

TABLE II
COMPARISON BETWEEN MASS FLOW RATES OF ANEMOMETER AND VOLUMETRIC MEASUREMENT AT APPROXIMATELY 85°F

Run No.	Flow Rate, cm^3/sec (Anemometer)	Flow Rate, cm^3/sec (Volumetric)	Deviation $\left(\frac{V - A}{V}\right)$, percent
1	16.0	15.7	-1.91
2	58.8	60.2	2.33
3	15.5	15.9	2.52
4	59.1	60.7	2.64
5	56.3	60.2	6.48
6	33.5	34.4	2.62
7	50.9	52.7	3.42
8	72.0	73.0	1.37
9	64.5	66.5	3.01
10	119.5	127.0	5.91

$$\sum_i \eta_i \frac{(V - A)}{\Sigma \eta_i} = 2.84 \text{ percent}$$

TABLE III
PERCENT OF ERROR IN DATA

β^*	Error, percent (Experimental - Theoretical)	Error, percent (Volumetric - Anemometer)	Error, percent (Experimental α_{cl})
0.440	0	2.52	~0
0.0892	1.81	2.62	0.44
0.0491	1.56	3.42	0.006
0.0295	7.39	1.37	0.017
0.0175	5.75	6.72	0.006

UNCLASSIFIED

Security Classification

DOCUMENT CONTROL DATA - R & D

(Security classification of title, body of abstract and indexing annotation must be entered when the overall report is classified)

1. ORIGINATING ACTIVITY *(Corporate author)*
Arnold Engineering Development Center
ARO, Inc., Operating Contractor
Arnold Air Force Station, Tennessee

2a. REPORT SECURITY CLASSIFICATION
UNCLASSIFIED

2b. GROUP
N/A

3. REPORT TITLE
EXPERIMENTAL INVESTIGATION OF LAMINAR FLOW DEVELOPMENT IN A RECTANGULAR CHANNEL USING A LASER ANEMOMETER

4. DESCRIPTIVE NOTES *(Type of report and inclusive dates)*
Final Report

5. AUTHOR(S) *(First name, middle initial, last name)*
W. T. Snyder and W. H. Goethert, ARO, Inc.

6. REPORT DATE	7a. TOTAL NO. OF PAGES	7b. NO. OF REFS
October 1969	27	6

8a. CONTRACT OR GRANT NO. F40600-69-C-0001
b. PROJECT NO. 4344
c. Program Element 65401F
d. Task 32

9a. ORIGINATOR'S REPORT NUMBER(S)
AEDC-TR-69-186

9b. OTHER REPORT NO(S) *(Any other numbers that may be assigned this report)*
N/A

10. DISTRIBUTION STATEMENT
This document has been approved for public release and sale; its distribution is unlimited.

11. SUPPLEMENTARY NOTES
Available in DDC.

12. SPONSORING MILITARY ACTIVITY
Arnold Engineering Development Center, Air Force Systems Command, Arnold AF Station, Tennessee 37389

13. ABSTRACT

Flow in the entrance region of a parallel plate channel has been theoretically investigated by others with little or no experimental verification. Presented here is a new method for the analysis which involves a linearization of the inertia terms and the introduction of a stretched axial coordinate. Solutions are obtained for the velocity distribution in an incompressible fluid which is valid from the duct inlet to the fully developed region. An experimental parallel plate channel was operated using water as the working fluid. Velocity profiles, on the basis of the stretched axial coordinate, were established with the use of a laser doppler velocimeter. These velocity profiles are compared with the theoretical profiles. A significant variation between the experimental and theoretical velocity is seen near the inlet of the channel.

DD FORM 1 NOV 65 1473

UNCLASSIFIED

Security Classification

14. KEY WORDS	LINK A		LINK B		LINK C	
	ROLE	WT	ROLE	WT	ROLE	WT
laminar flow						
channel flow						
incompressible flow						
anemometers						
lasers						
speed indicators						
velocity						